J. Fluid Mech. (1985), *vol.* 160, *pp.* 317–336
Printed in Great Britain

Stability of finite-amplitude interfacial waves. Part 2. Numerical results

By D. I. PULLIN
Department of Mechanical Engineering, University of Queensland, St Lucia, Qld 4067, Australia

AND R. H. J. GRIMSHAW
Department of Mathematics, University of Melbourne, Parkville, Vic 3052, Australia

(Received 2 April 1984 and in revised form 7 November 1984)

In the preceding paper (Grimshaw & Pullin 1985) we discussed the long-wavelength modulational instability of interfacial progressive waves in a two-layer fluid. In this paper we complement our analytical results by numerical results for the linearized stability of finite-amplitude waves. We restrict attention to the case when the lower layer is infinitely deep, and use the Boussinesq approximation. For this case the basic wave profile has been calculated by Pullin & Grimshaw (1983*a*, *b*). The linearized stability problem for perturbations to the basic wave is solved numerically by seeking solutions in the form of truncated Fourier series, and solving the resulting eigenvalue problem for the growth rate as a function of the perturbation wavenumber. For small or moderate basic wave amplitudes we show that the instabilities are determined by a set of low-order resonances. The lowest resonance, which contains the modulational instability, is found to be dominant for all cases considered. For higher wave amplitudes, the resonance instabilities are swamped by a local wave-induced Kelvin–Helmholtz instability.

1. Introduction

In the preceding paper (Part 1 – Grimshaw & Pullin 1985) we considered the long-wavelength modulational instability of small-amplitude interfacial waves propagating on the interface between two fluids of densities ρ_1 and ρ_2 and undisturbed depths d_1 and d_2 respectively. Our results showed that instability occurs within an instability band in the (p, q)-plane, where (p, q) is the modulation wavenumber. The configuration of the instability band is a function of the parameters ρ_1/ρ_2 and kd_1, kd_2, where k is the wavenumber of the basic wave. Various band configurations were identified, which are summarized in figure 1 of Part 1, while the dependence of the band configuration on the parameters is summarized in figure 6 of Part 1. In all cases the results pertain to that portion of the (p, q)-plane where p and q are $O(\delta)$. Here δ is a non-dimensional measure of the wave amplitude. The instability bandwidth is $O(\delta)$ and the growth rates are $O(\delta^2)$.

In this paper we complement the results of the modulational instability analysis by numerical calculations for the stability of finite-amplitude waves subject to modulations of finite wavenumber (p, q). In two previous papers (Pullin & Grimshaw 1983*a*, *b*) we calculated numerically the wave profiles for the special case when the lower layer is infinitely deep (i.e. $kd_2 \to \infty$), using the Boussinesq approximation (i.e. $\rho_2 \approx \rho_2$, except in the buoyancy terms). Results were obtained for a range of values

of the wave amplitude δ and the non-dimensional depth kd, and for a range of basic linear shear flows in the upper layer of the form $\bar{u}_1 - \Omega_1 y$. For the stability calculations we restrict attention to the case when there is no basic shear flow (i.e. $\bar{u}_1 = \Omega_1 = 0$). The steady waves are perturbed with an infinitesimal modulation of wavenumber (p, q), and we determine the resulting instabilities as functions of (p, q) and the wave parameters δ and kd_1. The stability analysis described here is based on the technique developed by McLean *et al.* (1981) (see also McLean 1982*a*, *b*) for the study of the instability of finite-amplitude surface gravity waves (i.e. $\rho_1 = 0$). Yuen (1983) has used the same technique to study the stability of interfacial waves when there is a basic current jump across the interface (i.e. $\bar{u}_1 \neq 0$, but $\Omega_1 = 0$), and each layer is infinitely deep (i.e. $kd_1, kd_2 \to \infty$).

In §2 we formulate the stability problem for finite-amplitude interfacial waves, and seek normal-mode solutions describing modulations of wavenumber (p, q) and growth rate s. The formulation and preliminary analysis is analogous to that described by McLean *et al.* (1981) and McLean (1982*a*, *b*) for surface gravity waves. In particular, we show that, for small wave amplitudes δ, instabilities will occur as a result of resonances. Each resonance can be regarded as the interaction of two sideband waves with N components of the basic wave. The $N = 1$ resonance does not exist, but all resonances exist for $N \geqslant 2$. In particular, the $N = 2$ resonance contains the modulational instability described in Part 1 (see the discussion in §5 of that paper). The numerical solution of the truncated eigenvalue problem is described in §3 and the results are presented in §4. Generally, our results have a qualitative similarity to the results for surface gravity waves. However, there are some differences; most notably, for small or moderate values of δ (the wave amplitude) the instability is dominated by the lowest-order resonance $N = 2$, but for larger values of δ this is swamped by the appearance of a local wave-induced Kelvin–Helmholtz (KH) instability. It is instructive to compare our results with those of Yuen (1983), who considered the stability of interfacial waves for the case when each fluid layer is infinitely deep (i.e. $kd_1, kd_2 \to \infty$) and the density ratio ρ_1/ρ_2 is either 0.1 or 0.9. He also included a basic current jump $\bar{u}_1$ across the interface. When $\bar{u}_1 = 0$ his results are comparable to ours. However, when $\bar{u}_1 \neq 0$, there is a short-wavelength KH instability for the undisturbed interface which persists for waves of small amplitude. This KH instability is distinct from the wave-induced KH instability calculated here. We also note from Yuen's results that the low-order resonance instabilities of relatively long wavelength persist when $\bar{u}_1 \neq 0$. Further discussion of our results is taken up in §5. In Appendix A we show that the Boussinesq approximation is dynamically self-consistent. In Appendix B we compare viscous attenuation of the wave amplitude with the instabilities calculated here, and show that for wave parameters appropriate to the oceanic pycnocline the viscous attenuation may be neglected.

2. Preliminary analysis

We shall consider finite-amplitude progressive waves on the interface between two incompressible and inviscid fluids. In coordinates (x, y, z) the basic wave has wavelength λ and propagates in the x-direction with speed c. Gravity g acts in the negative y-direction, while the fluid densities are ρ_1 and ρ_2 ($\rho_2 > \rho_1$), where subscripts 1 and 2 refer to fluid properties above and below the interface. The upper fluid is bounded above by a rigid plane at $y = d_1$ and the lower fluid is of infinite depth (i.e. $d_2 \to \infty$ in the notation of Part 1); the x-axis is the mean level of the wave. Pullin

& Grimshaw (1983*a*, *b*, henceforth referred to as PG) have described some of the properties of steady progressive waves using the Boussinesq approximation for the case when the upper fluid has a basic linear shear flow $\bar{u}_1 - \Omega_1 y$ with either $\bar{u}_1 = 0$ or $\Omega_1 = 0$. Here we propose to study the linearized stability of these waves for the case when the upper fluid has no basic flow (i.e. $\bar{u}_1, \Omega_1 = 0$). It is convenient to employ the same non-dimensionalization used in PG, which was also used in Part 1. We use the lengthscale λ/π and timescale $(\lambda/\pi\alpha g)^{\frac{1}{2}}$, where $\alpha = (\rho_2 - \rho_1)/(\rho_2 + \rho_1)$ is the Boussinesq parameter. As far as possible we shall use the notation used in PG. Thus we choose a frame of reference at rest with respect to the steady progressive wave. The dimensionless forms of $(x - ct, y, z, t, \Delta, \lambda, d_1, c, \rho_1, \rho_2)$ are $(X, Y, Z, T, \delta, \pi, D_1, C, 1-\alpha, 1+\alpha)$, where 2Δ is the crest-to-trough wave amplitude (note that $\Delta \approx 2|A|$, where $\epsilon|A|$ is the wave amplitude defined in Part 1, (4.5)).

The equations of motion have been described in Part 1 (see §2 and (2.1), (2.2)). Here we restrict attention to the Boussinesq approximation $\alpha \to 0$ (see Appendix A). In each fluid the flow is irrotational with a velocity potential Φ_j ($j = 1, 2$), and the velocity field $\boldsymbol{U}_j = (U_j, V_j, W_j) = \nabla\Phi_j$. At the upper boundary $Y = D_1$ we put $V_1 = 0$, while $V_2 \to 0$ as $Y \to -\infty$. It is shown in Appendix A that for $\alpha \to 0$ the rigid upper boundary is a dynamically self-consistent approximation to a free-surface upper boundary. The boundary conditions at the interface $Y = \eta(X, Y, T)$ are

$$\frac{\partial\eta}{\partial T} + U_j \frac{\partial\eta}{\partial X} + W_j \frac{\partial\eta}{\partial Z} = V_j \quad (j = 1, 2) \quad \text{on } Y = \eta, \tag{2.1a,b}$$

$$\frac{\partial\Phi_2}{\partial T} - \frac{\partial\Phi_1}{\partial T} + \tfrac{1}{2}(|\boldsymbol{U}_2|^2 - |\boldsymbol{U}_1|^2) + 2\eta = 0 \quad \text{on } Y = \eta. \tag{2.1c}$$

Next we let the steady plane progressive wave discussed in PG be denoted here by $\bar{\eta}(X)$ and $\bar{\Phi}(X, Y)$. We then linearize the equations of motion about this solution, and write

$$\eta = \bar{\eta}(X) + \eta'(X, Z, T), \tag{2.2a}$$

$$\Phi_j = \bar{\Phi}_j(X, Y) + \phi_j'(X, Y, Z, T) \quad (j = 1, 2), \tag{2.2b}$$

where $|\eta'| \ll |\bar{\eta}|$ and $|\phi_j'| \ll |\bar{\Phi}_j|$. The perturbed velocity potentials ϕ_j' satisfy Laplace's equation in each fluid, while the linearized boundary conditions are

$$\frac{\partial\eta'}{\partial T} + \bar{U}_j \frac{\partial\eta'}{\partial X} + u_j' \frac{\partial\bar{\eta}}{\partial X} + \eta' \left(\frac{\partial\bar{U}_j}{\partial Y}\frac{\partial\bar{\eta}}{\partial X} - \frac{\partial\bar{V}_j}{\partial Y}\right) - v_j' = 0 \quad (j = 1, 2) \quad \text{on } Y = \bar{\eta}, \tag{2.3a,b}$$

$$\frac{\partial\phi_2'}{\partial T} - \frac{\partial\phi_1'}{\partial T} + \bar{U}_2 u_2' + \bar{V}_2 v_2' - \bar{U}_1 u_1' - \bar{V}_1 v_1' + \eta' \left(2 + \bar{U}_2 \frac{\partial\bar{U}_2}{\partial Y} + \bar{V}_2 \frac{\partial\bar{V}_2}{\partial Y} - \bar{U}_1 \frac{\partial\bar{U}_1}{\partial Y} - \bar{V}_1 \frac{\partial\bar{V}_1}{\partial Y}\right) = 0 \quad \text{on } Y = \bar{\eta}, \tag{2.3c}$$

where $\boldsymbol{u}_j' = (u_j, v_j, w_j) = \nabla\phi_j'$ is the perturbed velocity field. It may be shown that, in the subsequent formulation of the eigenvalue problem, use of both equations (2.3*a*, *b*) leads to a degenerate system with concomitant infinite eigenvalues. Instead we use a single kinematic condition (2.3*a*) and introduce an auxiliary normal-velocity condition obtained by eliminating $\partial\eta'/\partial T$ from (2.3*a*, *b*). This is

$$(\bar{U}_1 - \bar{U}_2)\frac{\partial\eta'}{\partial X} + (u_1' - u_2')\frac{\partial\bar{\eta}}{\partial X} + \eta' \left\{\left(\frac{\partial\bar{U}_1}{\partial Y} - \frac{\partial\bar{U}_2}{\partial Y}\right)\frac{\partial\bar{\eta}}{\partial X} - \frac{\partial\bar{V}_1}{\partial Y} + \frac{\partial\bar{V}_2}{\partial Y}\right\} - v_1' + v_2' = 0 \quad \text{on } Y = \bar{\eta}. \tag{2.4}$$

We follow the approach used by McLean *et al.* (1981) and McLean (1982*a*, *b*) and seek a solution of the form

$$\eta' = \exp\{ST + \mathrm{i}(PX+QZ)\} \sum_{-\infty}^{\infty} a_m \exp(2\mathrm{i}mX), \tag{2.5a}$$

$$\phi_1' = \exp\{ST + \mathrm{i}(PX+QZ)\} \sum_{-\infty}^{\infty} b_m \exp(2\mathrm{i}mX) \frac{\cosh[R_m(D_1 - Y)]}{\cosh[R_m D_1]}, \tag{2.5b}$$

$$\phi_2' = \exp\{ST + \mathrm{i}(PX+QZ)\} \sum_{-\infty}^{\infty} c_m \exp(2\mathrm{i}mX) \exp[R_m Y], \tag{2.5c}$$

where

$$R_m = [(2m+P)^2 + Q^2]^{\frac{1}{2}}. \tag{2.5d}$$

The physical disturbance corresponds to the real part of (2.5*a*–*c*). Here P, Q are arbitrary real numbers and the proposed solution (2.5*a*–*c*) describes a modulation whose wavenumber is (P, Q) and whose growth rate is the complex number S (compare Part 1, §4). Once the steady wave $\bar{\eta}$, $\bar{\Phi}_j$ is known, substitution of (2.5*a*–*c*) into (2.3*a*, *b*) and (2.4) yields an eigenvalue problem for the complex coefficients (a_m, b_m, c_m) and the eigenvalue S. Instability corresponds to $\mathrm{Re}\,(S) > 0$, and the aim of the analysis is to determine the instability as a function of (P, Q) and the parameters δ and D_1 which describe the steady progressing wave. The numerical solution of this eigenvalue problem is described in §3; in the remainder of this section we present some preliminary analysis pertaining to the limit $\delta \to 0$, where we recall that δ is the amplitude of the steady progressive wave. The analysis is analogous to that developed by McLean *et al.* (1981) and McLean (1982*a*, *b*) for surface gravity waves.

When $\delta = 0$ the steady progressive wave is $\bar{\eta} = 0, \bar{\Phi}_j = -C_0 X$, where C_0 is the phase speed for an infinitesimal steady progressing wave, and is given by (see Part 1, or PG)

$$C_0 = (1 + \coth 2D_1)^{-\frac{1}{2}}. \tag{2.6}$$

In this limit the eigenfunctions and eigenvalues are

$$\eta_n' = \exp\{S_n T + \mathrm{i}((P+2n)X + QZ)\}, \tag{2.7a}$$

$$S_n = -\mathrm{i}\sigma_n, \quad \sigma_n = -C_0(P+2n) + W(P+2n, Q), \tag{2.7b}$$

where

$$W(P,Q) = \pm \left\{\frac{2R}{1+\coth RD_1}\right\}^{\frac{1}{2}}, \quad R = (P^2+Q^2)^{\frac{1}{2}}. \tag{2.7c}$$

Here the sign of W is chosen so that $W(P, Q) = -W(-P, -Q)$. These eigenfunctions are just infinitesimal waves with wavenumber $\boldsymbol{k} = (k, l) = (P+2n, Q)$. Their frequencies are $-kC_0 + W(\boldsymbol{k})$, which corresponds to the linear dispersion relation in a frame of reference moving with speed C_0. Note that there is a degeneracy in the choice of P since $\sigma_n(P, Q) = \sigma_{n+1}(P-2, Q)$. The degeneracy is a consequence of the representation (2.5*a*–*c*). Following McLean (1982*a*, *b*), we will label the eigenfunctions by (P, Q) and specify the index of the dominant coefficient a_n; this fixes the dominant wavenumber $\boldsymbol{k} = (P+2n, Q)$.

For small δ, instabilities arise whenever two of these linear modes satisfy the resonance condition

$$\sigma_n(P, Q) = \sigma_{n+N}(P, Q) \tag{2.8}$$

for specified P, Q and some integers n, N with $N > 0$. This resonance condition is readily interpreted in a fixed frame of reference where the linear dispersion relation is $\omega = W(\boldsymbol{k})$. We define $\boldsymbol{k}_1 = (P+2n, Q)$, $\boldsymbol{k}_2 = (P+2n+2N, Q)$ and $\boldsymbol{k}_0 = (2, 0)$, where

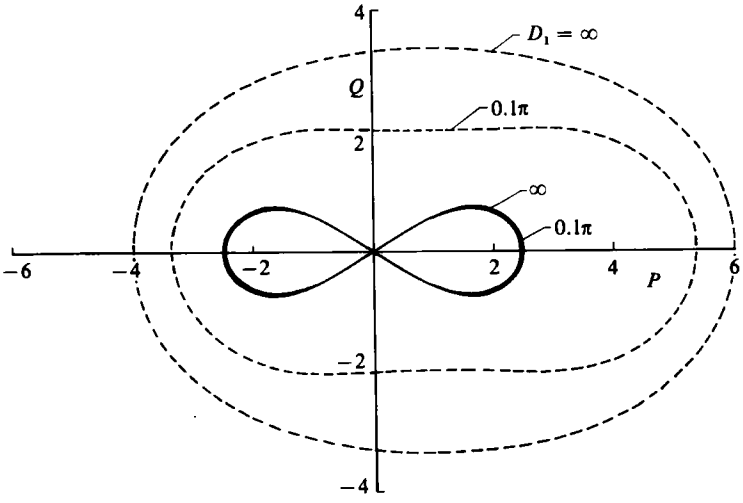

FIGURE 1. Resonance curves (stability bands, $\delta = 0$), $\alpha = 0$, $D_2 \to \infty$. Values of D_1 shown. ——, $N = 2$; – – –, $N = 3$.

the index zero corresponds to the steady progressing wave; similarly we define $\omega_1 = W(\boldsymbol{k}_1)$, $\omega_2 = W(\boldsymbol{k}_2)$ and $\omega_0 = W(\boldsymbol{k}_0)$. The resonance condition (2.8) then becomes

$$\boldsymbol{k}_2 - \boldsymbol{k}_1 = N\boldsymbol{k}_0, \quad \omega_2 - \omega_1 = N\omega_0. \tag{2.9}$$

Note that without loss of generality ω_0 can be taken positive, but $\omega_{1,2}$ can take either sign. The lowest-order resonance is $N = 1$ and corresponds to a triad resonance. However, for the interfacial waves being considered here it can be shown that the group velocity V is always less than the phase speed C in absolute value. By using arguments similar to those employed for surface gravity waves (see Phillips 1960) it may be shown that with $N = 1$ the resonance condition (2.9) cannot be met.

The next resonance is $N = 2$ and corresponds to a special case of a quartet resonance (see Yuen & Lake 1982). It can now be shown that the resonance condition (2.9) can be met with $\omega_1 < 0$ and $\omega_2 > 0$. The resonance condition generates a curve in the (P, Q)-plane, and this is shown in figure 1 for two values of D_1. The resonance curve is a figure-of-eight very similar to the resonance curve obtained for surface gravity waves (Phillips 1960). Significantly, the resonance curve passes through the origin of the (P, Q)-plane, and near the origin the instability reduces to the long-wavelength modulational instability discussed in Part 1 (§5). Further, all the higher-order resonances $N \geqslant 3$ exist; the resonance curve for $N = 3$ is shown in figure 1. We expect that the growth rates associated with these resonances are $O(\delta^N)$ (McLean 1982*a*, *b*; Yuen & Lake 1982). Also we note that the resonance curves are symmetrical about $P = -2n - N$ and $Q = 0$. Using the degeneracy in the choice of P and n discussed above, we follow McLean (1982*a*, *b*) and choose $n = -\frac{1}{2}N$ for even N, and $n = -\frac{1}{2}(N+1)$ for odd N. With this choice the resonance curves are symmetrical about $P = 0$, $Q = 0$ for even N, and symmetrical about $P = 1$, $Q = 0$ for odd N. The resonance condition (2.9) thus becomes

$$\left.\begin{aligned} \sigma^-_{-\frac{1}{2}N}(P, Q) &= \sigma^+_{\frac{1}{2}N}(P, Q) \quad \text{for even } N, \\ \sigma^-_{-\frac{1}{2}(N+1)}(P, Q) &= \sigma^+_{\frac{1}{2}(N-1)}(P, Q) \quad \text{for odd } N. \end{aligned}\right\} \tag{2.10}$$

Here the superscript $\pm$ corresponds to the choice of sign in (2.7*c*) and corresponds to $\omega_2 > 0$ and $\omega_1 < 0$.

3. Numerical analysis

Numerical solutions for the stability characteristics of interfacial waves with finite wave amplitude δ are now obtained as follows. First, we consider the calculation of the required properties of the basic wave. From the numerical solutions of PG, the wave profile and the velocity of each fluid at the interface may be expressed in the form

$$z(e) = X(e) + \mathrm{i}\bar{\eta}(e) = e + \sum_{n=0}^{N-1} [A_n \sin(2ne) + \mathrm{i}B_n \cos(2ne)], \tag{3.1a}$$

$$\bar{U}_j(e) - \mathrm{i}\bar{V}_j(e) = \sum_{n=0}^{N} [F_n^{(j)} \cos(2ne) - \mathrm{i}G_n^{(j)} \sin(2ne)] \quad (j = 1, 2). \tag{3.1b}$$

Here e is an interfacial parameter which varies over the range 0 to π. The coefficients A_n, B_n together with a further set of coefficients for the velocity jump at the interface are determined in PG from the kinematic and dynamic boundary conditions at the interface $Y = \bar{\eta}$. The coefficients $F_n^{(j)}$, $G_n^{(j)}$ are then obtained by fitting a truncated Fourier series to the respective velocity components at the interface, using equation (40) of PG*a*. For the basic-wave solutions considered here N was increased within the range $15 \leqslant N \leqslant 60$ until $|A_N|$, $|B_N|$ were $O(10^{-15})$ in 14 digit arithmetic. An exception to this was $D_1 = 0.1\pi$, $\delta = 0.05\pi$, where $|A_{60}|$, $|B_{60}|$ were $O(10^{-12})$. All properties of the basic wave that appear in (2.3) and (2.4) may be readily obtained from (3.1).

Next we truncate the infinite series in (2.5*a–c*) to finite series over the range $-M \leqslant m \leqslant M$ and substitute the truncated series into (2.3*a*, *c*) and (2.4). The resulting equations are now satisfied at $2M+1$ points on a single wavelength, $0 \leqslant X \leqslant \pi$, of the basic wave, chosen to give equal chordlength spacing along the wave interface:

$$s_j = \frac{jL_M}{2M+2}, \quad L_M = \sum_{j=1}^{2M+2} [(X_j - X_{j-1})^2 + (\bar{\eta}_j - \bar{\eta}_{j-1})^2]^{\frac{1}{2}},$$

and $j = 1, \ldots, 2M+1$. This leads to $6M+3$ equations, which may be written in matrix form as

$$\boldsymbol{A}_1[\boldsymbol{a}, \boldsymbol{b}] + \boldsymbol{A}_2[\boldsymbol{c}] = S\{\boldsymbol{B}_1[\boldsymbol{a}, \boldsymbol{b}] + \boldsymbol{B}_2[\boldsymbol{c}]\}, \tag{3.2a}$$

$$\boldsymbol{C}[\boldsymbol{c}] = \boldsymbol{D}[\boldsymbol{a}, \boldsymbol{b}]. \tag{3.2b}$$

Here $\boldsymbol{A}_1$, $\boldsymbol{B}_1$ are $(4M+2) \times (4M+2)$ complex matrices, $\boldsymbol{A}_2$, $\boldsymbol{B}_2$ are $(4M+2) \times (2M+1)$ complex matrices, $\boldsymbol{C}$ is a $(2M+1) \times (2M+1)$ complex matrix, and $\boldsymbol{D}$ is a $(2M+1) \times (4M+2)$ complex matrix. Their elements are determined from the procedure described above. Further, $[\boldsymbol{a}, \boldsymbol{b}]$ is a column vector with components $\{a_{-M}, \ldots, a_M, b_{-M}, \ldots, b_M\}$ and $[\boldsymbol{c}]$ is a column vector with components $\{c_{-M}, \ldots, c_M\}$. Premultiplying (3.2*b*) by $\boldsymbol{C}^{-1}$ and substituting into (3.2*a*) gives the $(4M+2) \times (4M+2)$ eigenvalue problem

$$(\boldsymbol{A}_1 + \boldsymbol{A}_2 \boldsymbol{C}^{-1} \boldsymbol{D})[\boldsymbol{a}, \boldsymbol{b}] = S(\boldsymbol{B}_1 + \boldsymbol{B}_2 \boldsymbol{C}^{-1} \boldsymbol{D})[\boldsymbol{a}, \boldsymbol{b}] \tag{3.3}$$

with eigenvalue S and eigenvector $[\boldsymbol{a}, \boldsymbol{b}]$. Using the symmetry properties of the basic wave it may be shown that, if S and $[\boldsymbol{a}, \boldsymbol{b}]$ comprise a solution of (3.3), then so do $-S^*$ and $[-\boldsymbol{a}^*, \boldsymbol{b}^*]$. Hence the eigenvalues are either pure imaginary or occur in conjugate pairs. Instability thus corresponds to the existence of an eigenvalue with $\mathrm{Re}(S) \neq 0$.

The numerical procedure is as follows:

(i) Given D_1, δ, first calculate the basic wave from (3.1*a*, *b*);

(ii) fix (P, Q) and calculate the matrices in (3.2*a*, *b*);

(iii) determine $\boldsymbol{C}^{-1}$ and perform the matrix operations in (3.3);

(iv) solve the eigenvalue problem (3.3).

This last step was done using a version of the QZ-algorithm due to Garbow (1978). In some cases, the calculations were checked by results based on an LZ-algorithm (Kaufman 1975). All computations were performed in 14 digit arithmetic on a VAX 11/780 computer. Each calculation produces a set of $4M+2$ eigenvalues. An index m was assigned to each member corresponding to $\max|a_m|$ in the corresponding eigenvector. By tracking eigenvalue trajectories for $\delta > 0$ in the complex plane from the known value when $\delta = 0$, $S_m^{\pm}$ (2.7*b*, *c*), this index was verified and a branch sign ($\pm$) determined. Here we recall that $\pm$ refers to the choice of sign in (2.7*c*). Instability as δ increased from zero always occurred when the imaginary parts of distinct eigenvalues coalesced, in agreement with (2.10), and the eigenvalues then formed a conjugate pair. The boundaries of the instability bands were determined using various strategies based on the convergence of the imaginary parts of the appropriate resonant pair.

A difficulty encountered with this procedure as δ increased was the appearance of very large values of $\mathrm{Re}(S_m^{\pm})$ for $|m| \to M$. When $\mathrm{Re}(S)$ is plotted as a function of m these exceptionally large values of $\mathrm{Re}(S_m^{\pm})$ appeared in the spectrum tail, bounding a central band which was stable except for the resonant pairs (see figure 10). The central bandwidth decreased to a limiting width, which was independent of M above a threshold value, for large values of δ. We believe that this divergence is physically based, and can be interpreted as the onset of a local wave-induced KH instability due to the velocity jump across the interface. This is discussed further in §4.

Most of our calculations were carried out for the cases $D_1 \to \infty$, $D_1 = 0.25\pi$ and $D_1 = 0.1\pi$, with M in the range $10 \leqslant M \leqslant 32$. In terms of the modulational instability discussed in Part 1, these cases correspond to instability band configurations of case A, case A and case C respectively (see figure 6(*a*) of Part 1). The results of Part 1 give a transition from case A to B at $D_1 = 0.24\pi$, a further transition to case C at $D_1 = 0.19\pi$, and finally a transition to case B again at $D_1 = 0.033\pi$. Some calculations were attempted for a long wave with $D_1 = 0.01\pi$, but these were unsuccessful owing to resolution problems. For each D_1, $\delta = 0.01\pi$, 0.025π, 0.05π, 0.075π, ..., $\max(\delta)$; here $\max(\delta)$ is that value in the sequence beyond which satisfactory convergence (with $10 \leqslant M \leqslant 32$) could not be achieved owing to the difficulty discussed above. The values of $\max(\delta)$ may be compared with $\delta_{\max}$, the maximum amplitude of the basic wave found in PG. Thus for $D_1 \to \infty$ we find $\max(\delta) = 0.075\pi$, while $\delta_{\max} = 0.188\pi$; for $D_1 = 0.025\pi$ we find $\max(\delta) = 0.075\pi$ while $\delta_{\max} = 0.14\pi$; for $D_1 = 0.1\pi$ we find $\max(\delta) = 0.05\pi$ while $\delta_{\max} = 0.096\pi$. Thus only waves of moderate amplitude could be treated.

4. Results

The main results of our numerical calculations for the $N = 2$ and $N = 3$ instabilities are shown graphically in figures 2–8. The maximum growth rates for each of these bands are shown in tables 1–3. For small δ the bandwidth for the $N = 2$ instability (see figures 2, 4, 6 and 8) is $O(\delta)$, and the growth rates are $O(\delta^2)$. This is in agreement with the modulational instability discussed in Part 1.

For the case $D_1 \to \infty$ the $N = 2$ instability bands are shown in figure 2 and the $N = 3$ instability bands in figure 3. The maximum growth rate for the $N = 2$ instability (see table 1) is always for a two-dimensional disturbance (i.e. for a disturbance aligned with the basic wave direction). There is no evidence of a rapid shrinking of the $N = 2$

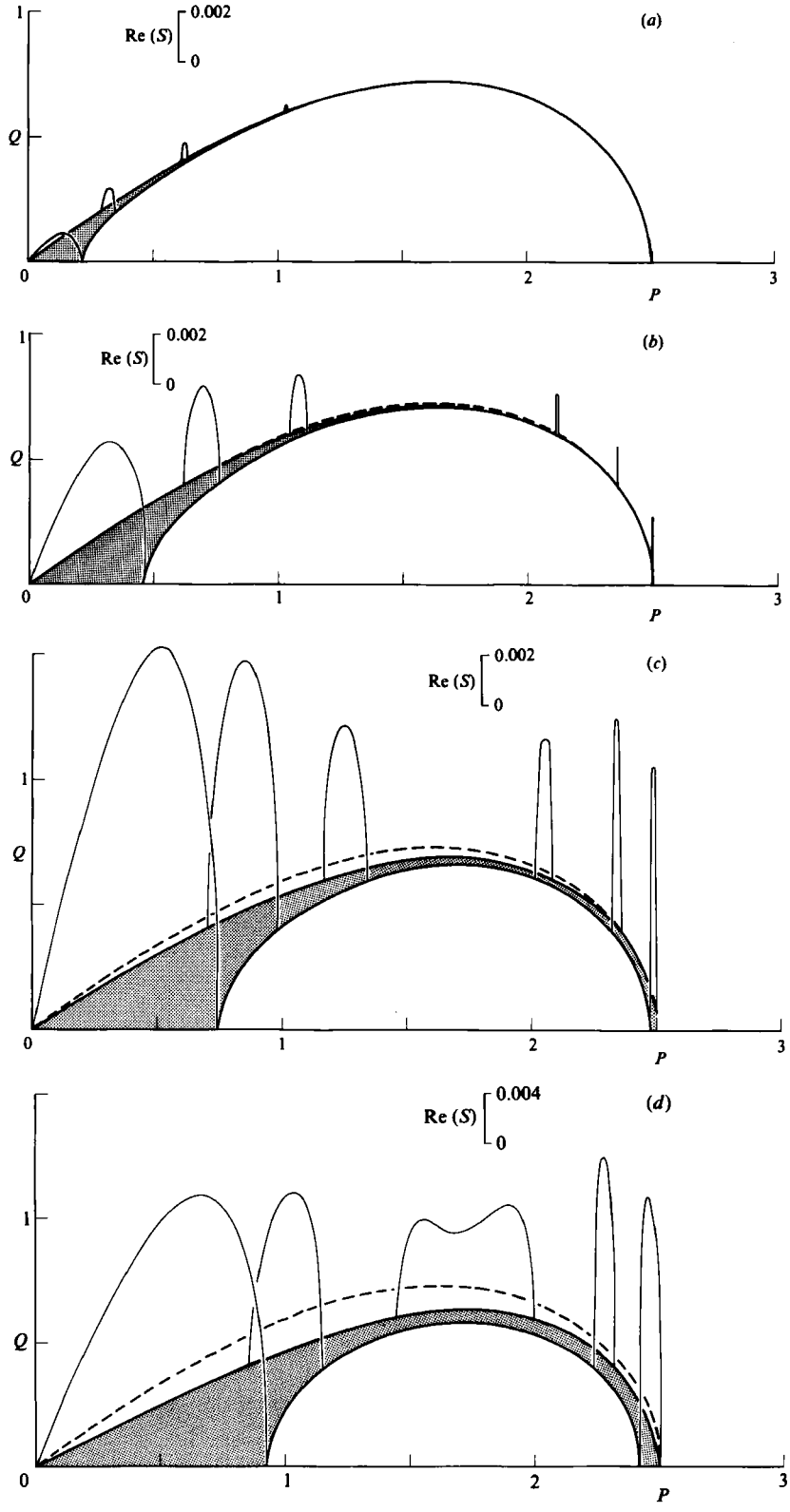

FIGURE 2. Stability diagrams with superposed growth rates (at Q = constant) for $N = 2$ instability, $D_1 \to \infty$; shaded regions are unstable bands; ---, resonance curve (instability band $\delta = 0$). (*a*) $\delta = 0.01\pi$; (*b*) 0.025π; (*c*) 0.05π; (*d*) 0.075π. Note different growth-rate scale for (*d*).

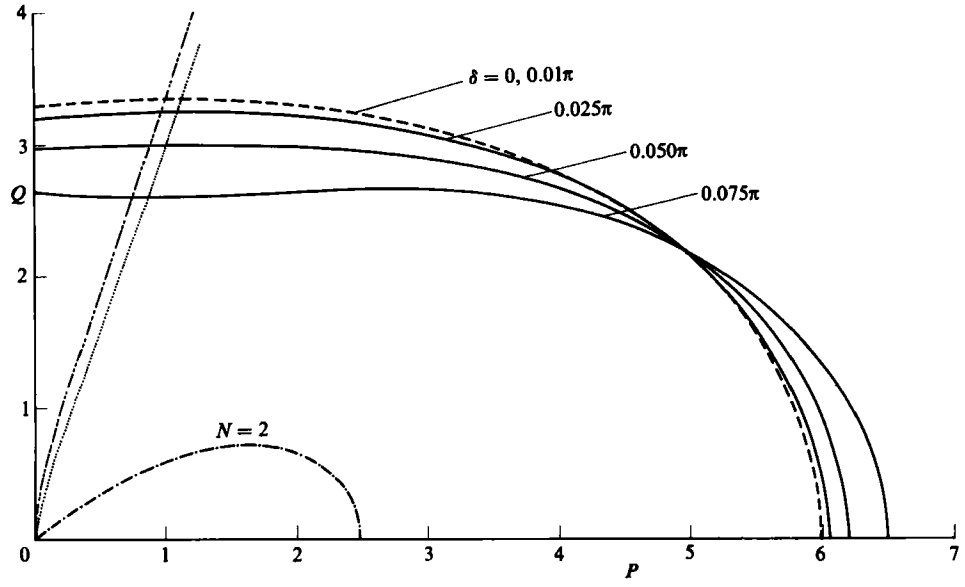

FIGURE 3. Stability diagram for $N = 3$ instability, $D_1 \to \infty$. ——, $N = 3$ resonance curve; - - - -, instability bands; values of δ indicated; ·—·, $N = 2$ resonance curve; ··—··, $S = 0$ ($\delta = 0$); · · · ·, $S = 0$ ($\delta = 0.05\pi$).

	$N = 2$				$N = 3$	
δ/π	P	Q	Re (S)	Im (S)	P	Q
0.01	0.15	0	1.17×10^{-3}	5.28×10^{-2}	1	3.3381
0.025	0.33	0	5.72×10^{-3}	1.139×10^{-1}	1	3.2560
0.050	0.52	0	1.52×10^{-2}	1.688×10^{-1}	1	2.9873
0.075	0.65	0	2.18×10^{-2}	1.921×10^{-1}	1	2.6034

TABLE 1. Maximum growth rate Re (S) for $N = 2$ instability band, $D_1 \to \infty$. Entries for $N = 3$ show position of instability band near point of probable max [Re (S)]. This band was not detected explicitly.

instability band with increasing δ, similar to that found by McLean *et al.* (1981) and McLean (1982*a*) for surface gravity waves in deep water. Yuen (1983) examined the stability of interfacial waves for the case when there is a basic current jump $\bar{u}_1$ across the interface and the density ratio ρ_1/ρ_2 is 0.1 or 0.9. Our parameter space comes closest to that studied by Yuen in figure 2(*b*), which corresponds to the case $N = 2$, $\rho_1/\rho_2 = 0.9$, $\bar{u}_1 = 0$, $\delta/\pi \approx 0.032$ in Yuen's figure 4(*d*). We find that there is good agreement in the calculated shape of the $N = 2$ instability band. In our calculations the $N = 3$ instability bands were not detected explicitly. The curves shown in figure 3 were inferred by tracking the convergence of Im $(S_1^+) \leftrightarrow$ Im (S_{-2}^-) from both sides. We estimate that the bandwidth in the (P, Q)-plane does not exceed 10^{-5} even for max $(\delta) = 0.075\pi$. It is evident that the $N = 3$ instability is insignificant.

The case $D_1 = 0.25\pi$ is shown in figure 4 ($N = 2$), figure 5 ($N = 3$) and table 2. This case is close to the value $D_1 = 0.24\pi$ at which the modulational-instability theory of Part 1 predicts a transition from case A to case B. This evidently accounts for the lower growth rates and narrower bandwidth for the $N = 2$ instability with long-

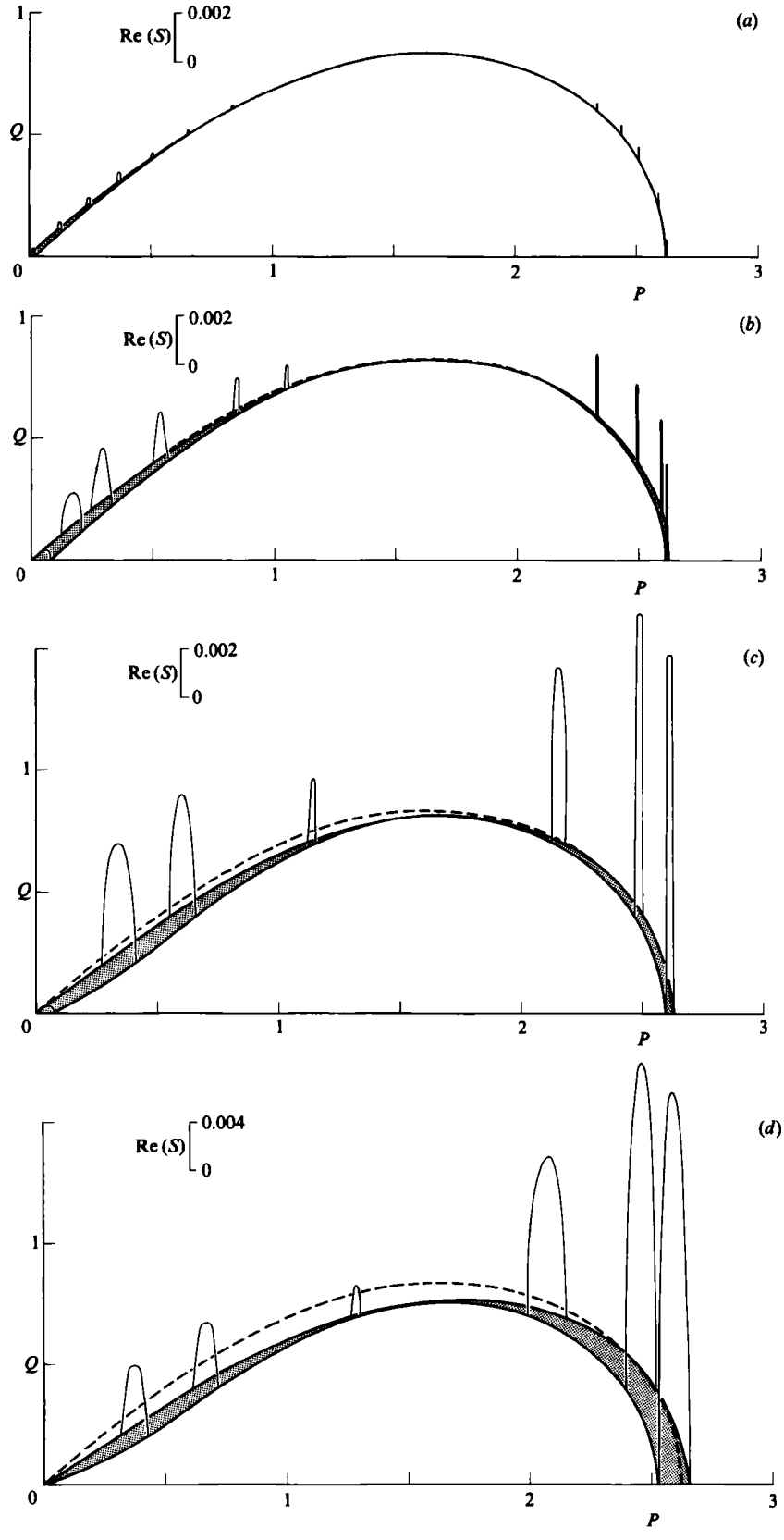

FIGURE 4. Stability diagrams with superposed growth rates (at Q = constant) for $N = 2$ instability, $D_1 = 0.25\pi$. (*a*) $\delta = 0.01\pi$; (*b*) 0.025π; (*c*) 0.05π; (*d*) 0.075π.

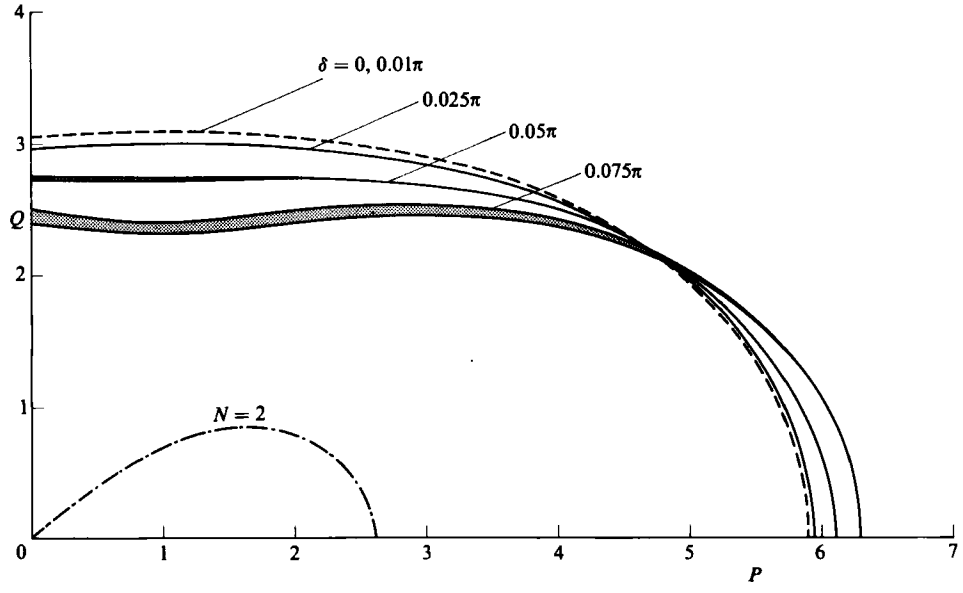

FIGURE 5. Stability diagram for $N = 3$ instability, $D_1 = 0.25\pi$. ---, $N = 3$ resonance curves; shaded areas are instability bands; values of δ indicated; ·—·, $N = 2$ resonance curve.

	$N = 2$				$N = 3$			
δ/π	P	Q	Re (S)	Im (S)	P	Q	Re (S)	Im (S)
0.010	2.617	0	6.4×10^{-4}	1.045	1	3.0803	3×10^{-5}	10^{-5}
0.025	2.610	0	3.95×10^{-3}	1.044	1	3.002	4.7×10^{-4}	10^{-8}
0.050	2.610	0	1.49×10^{-2}	1.039	1	2.746	3.58×10^{-3}	10^{-5}
0.075	2.590	0	3.28×10^{-2}	1.000	1	2.361	1.06×10^{-2}	10^{-4}

TABLE 2. Maximum growth rate Re (S) for $N = 2$ and $N = 3$ instability bands, $D_1/\pi = 0.25$

wavelength modulations (i.e. P, Q very small) when compared with other cases for the same value of δ. The maximum growth rate is still for a two-dimensional disturbance, but now occurs near the extremity of the figure-eight resonance curve (given by $P = 2.6169$). As δ increases, the long-wavelength modulation instability near the (P, Q)-origin is transformed from a two-dimensional instability (case A) to a transverse instability (case B); the transition occurs for $0.05\pi < \delta < 0.075\pi$. The $N = 3$ instability bands have a bandwidth $O(\delta^2)$ for small δ, and a growth rate of $O(\delta^3)$. For all δ considered, it is a weaker instability than the $N = 2$ instability.

The case $D_1 = 0.1\pi$ is shown in figure 6 ($N = 2$), figure 7 ($N = 3$) and table 3. The long-wavelength modulational instability in the $N = 2$ instability corresponds to case C of Part 1. The maximum growth rates now occur for a transverse modulation. The $N = 3$ instability bands again have growth rates $O(\delta^3)$, but are substantially larger than the corresponding growth rates for the case $D_1 = 0.25\pi$. However, the $N = 3$ instability is still weaker than the $N = 2$ instability.

In figure 8 we show one calculation for the $N = 2$ instability when $D_1 = 0.05\pi$ with $\delta = 0.01\pi$. Like the case $D_1 = 0.1\pi$ this is also a case-C modulational instability, but now the growth rates of the transverse instability are substantially larger for the same value of δ (see figure 6*a*).

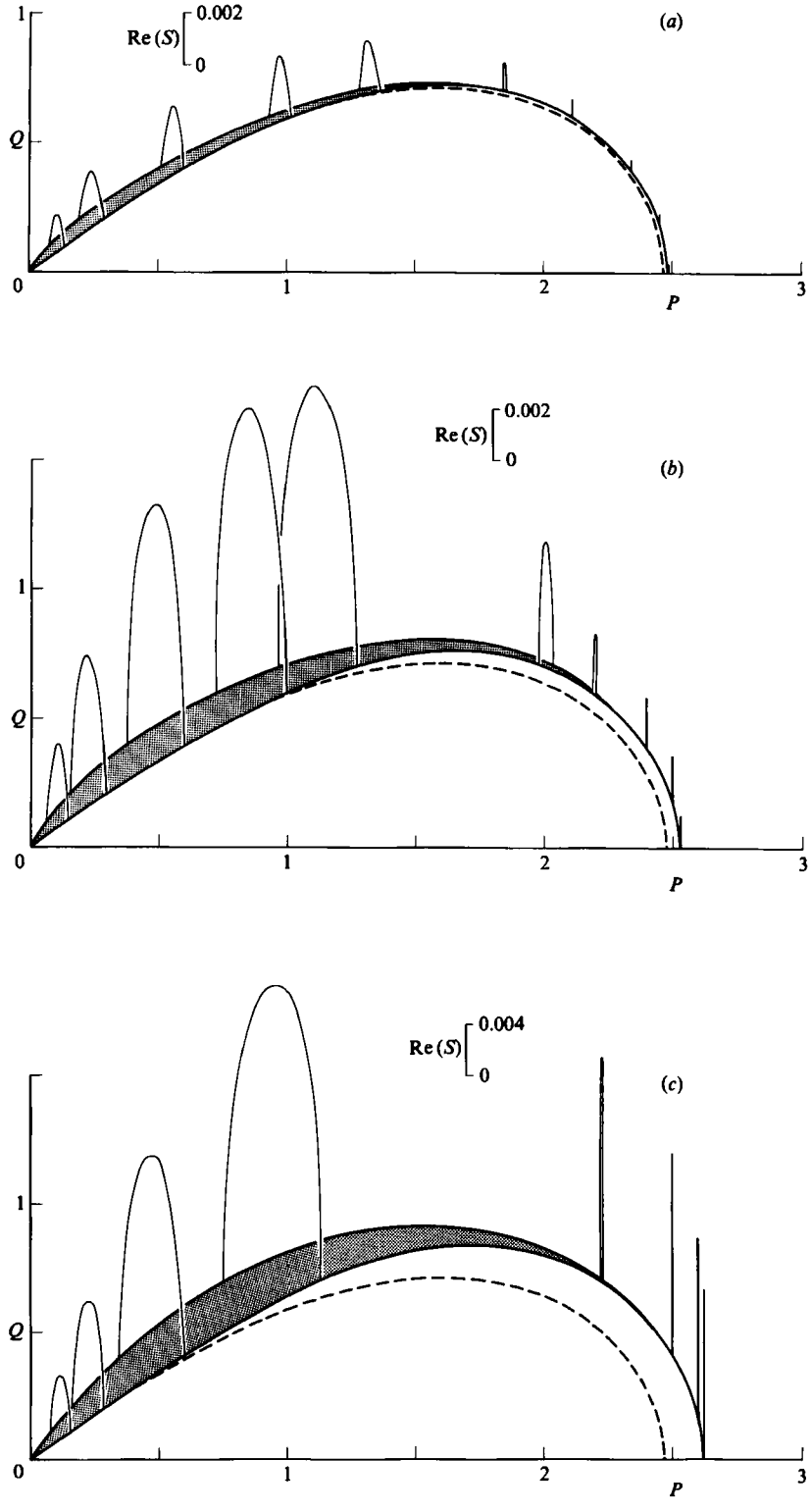

FIGURE 6. Stability diagrams with superposed growth rates (at Q = constant) for $N = 2$ instability, $D_1 = 0.1\pi$. (*a*) $\delta = 0.01\pi$; (*b*) 0.025π; (*c*) 0.050π.

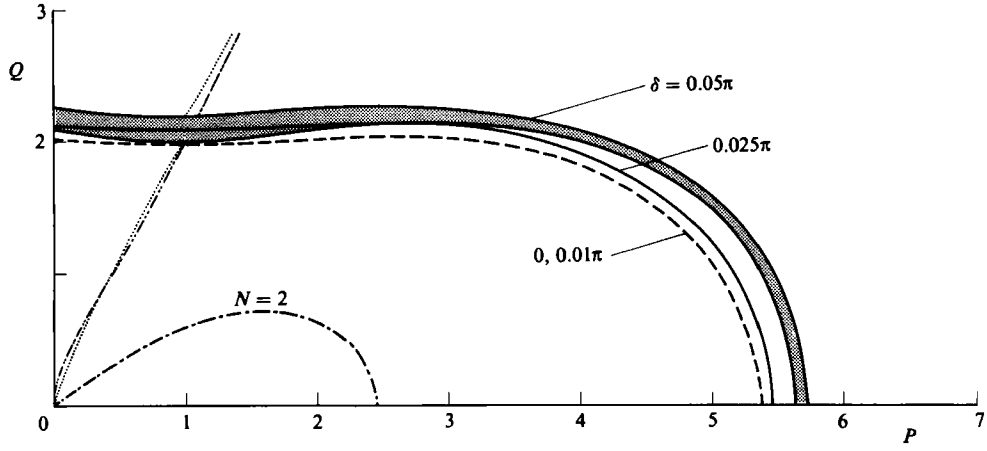

FIGURE 7. Stability diagram for $N = 3$ instability, $D_1 = 0.1\pi$. ---, $N = 3$ resonance curve; shaded areas are instability bands; values of δ indicated; ·—·, $N = 2$ resonance curve; ··—··, $S = 0$ ($\delta = 0$); ····, $S = 0$ ($\delta = 0.05\pi$).

	$N = 2$				$N = 3$			
δ/π	P	Q	Re (S)	Im (S)	P	Q	Re (S)	Im (S)
0.01	0.70	0.480	2.37×10^{-3}	1.193×10^{-1}	1	1.981	1.1×10^{-4}	10^{-5}
0.025	0.95	0.638	1.10×10^{-2}	1.897×10^{-1}	1	2.049	2.81×10^{-3}	10^{-7}
0.050	1.20	0.810	2.41×10^{-2}	2.970×10^{-1}	1	2.110	2.11×10^{-2}	10^{-4}

TABLE 3. Maximum growth rate Re (S) for $N = 2$ and $N = 3$ instability bands, $D_1/\pi + 0.10$

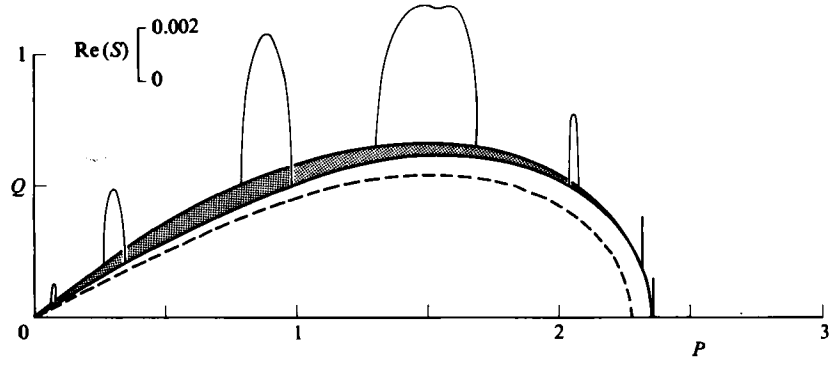

FIGURE 8. Stability diagram for $N = 2$ instability, $D_1 = 0.05\pi$, $\delta = 0.01\pi$.

In figures 3 and 7 we show the $S = 0$ trajectory in the (P, Q)-plane for $\delta = 0, 0.05\pi$ for the cases $D_1 \to \infty$ and $D_1 = 0.1\pi$ respectively. Disturbances with $S = 0$ are steady in the frame of reference of the basic wave, and for rational values of (P, Q) represent possible bifurcations of the basic wave to steady periodic wave patterns. Such bifurcations have been found for surface gravity waves in deep water by Chen & Saffman (1980) in the two-dimensional case, and by Saffman & Yuen (1980) and Meiron, Saffman & Yuen (1982) in the three-dimensional case (see also Yuen & Lake 1982). Here the $S = 0$ trajectory remains attached to the origin of the (P, Q)-plane

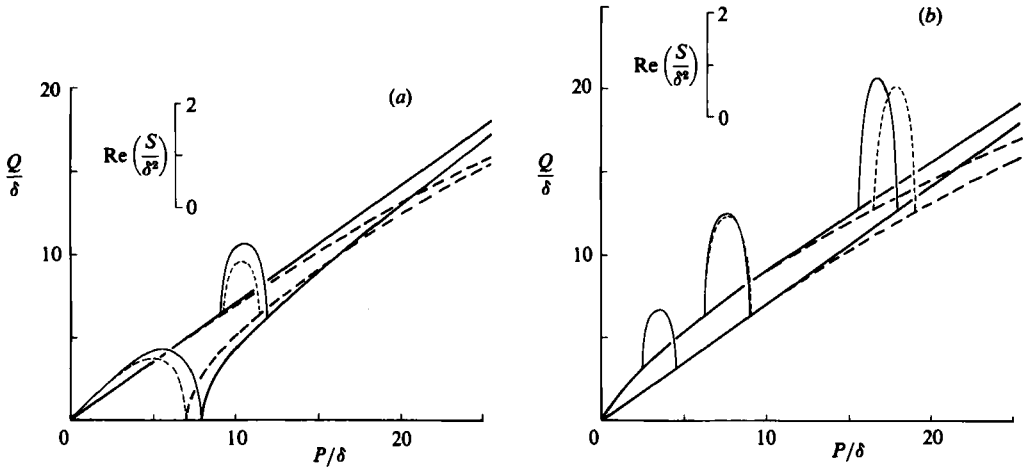

FIGURE 9. Stability boundaries and superposed growth rates (at Q = constant), (*a*) $D_1 \to \infty$; (*b*) $D_1 = 0.1\pi$. ——, modulational instability; – – –, numerical, $\delta = 0.01\pi$.

(the full trajectory is symmetric about the line $P = 1$, but the second branch has not been displayed). Hence we may conclude that there are no steady two-dimensional bifurcations for the range $0 \leqslant \delta \leqslant \max(\delta)$. There are, of course, an infinite set of three-dimensional bifurcations.

In figure 9 we compare the numerical results with the modulational-instability calculations of Part 1. For the case $D_1 \to \infty$, $\delta = 0.01\pi$ (figure 9*a*) the modulational-instability calculations overpredict the bandwidth and growth rate. However, for the case $D_1 = 0.1\pi$, $\delta = 0.01\pi$ (figure 9*b*) there is good agreement.

We next give arguments to support the hypothesis that the spectrum divergence at large m can be attributed to local wave-induced KH instability (see the discussion at the end of §3). Consider the stability of a flat, infinite vortex sheet with local velocity difference $\overline{U}_1 - \overline{U}_2$, and inclined to the horizontal at an angle θ. We consider the case $D_1 \to \infty$ for simplicity. Using the same notation employed in §2 (see (2.5*a–d*)), the linearized dispersion relation is

$$S_m^{\pm} = \tfrac{1}{2}[-\mathrm{i}(2m+P)(\overline{U}_1+\overline{U}_2) \pm \{(2m+P)^2(\overline{U}_1-\overline{U}_2)^2 - 4R_m\cos\theta\}^{\frac{1}{2}}]. \tag{4.1}$$

For $|2m+P| < k_c$ the vortex sheet is stable, where k_c satisfies the relation

$$k_c^2(\overline{U}_1-\overline{U}_2)^2 = 4\cos\theta\{k_c^2+Q^2\}^{\frac{1}{2}}. \tag{4.2}$$

Otherwise the vortex sheet is unstable. Putting $k_c = |2m_c+P|$ with $m_c > 0$, we see that m_c is effectively a threshold index for the onset of KH instability. For the cases considered here $k_c \gg |P|$, and hence there is local KH instability for $|m| \geqslant m_c$. For the basic wave we now identify $\overline{U}_1$, $\overline{U}_2$ as the local fluid speed at the interface, and put $\cos\theta = (1+\bar{\eta}_x^2)^{-\frac{1}{2}}$, and evaluate (4.2) at that point on the interface where $\cos\theta\,(\overline{U}_1-\overline{U}_2)^{-2}$ is a minimum. This always occurred at the wave crest. In figure 10 we show a plot of the continuous $\mathrm{Re}\,(S_m)$ spectrum so obtained from (4.1), and compare this with the calculated discrete spectrum for $\delta = 0.05\pi$ at three values of (P, Q). Note that only the case $P = 0.5$, $Q = 0$ (figure 10*a*) contains an eigenvalue corresponding to an $N = 2$ instability. There is reasonable agreement with the value of m_c. For $|m| > m_c$ the predicted values of $\mathrm{Re}\,(S_m)$ overestimate the calculated values. This is probably because the expression (4.1) is the result of a local analysis and takes no account of wave curvature and the dynamical properties of the basic

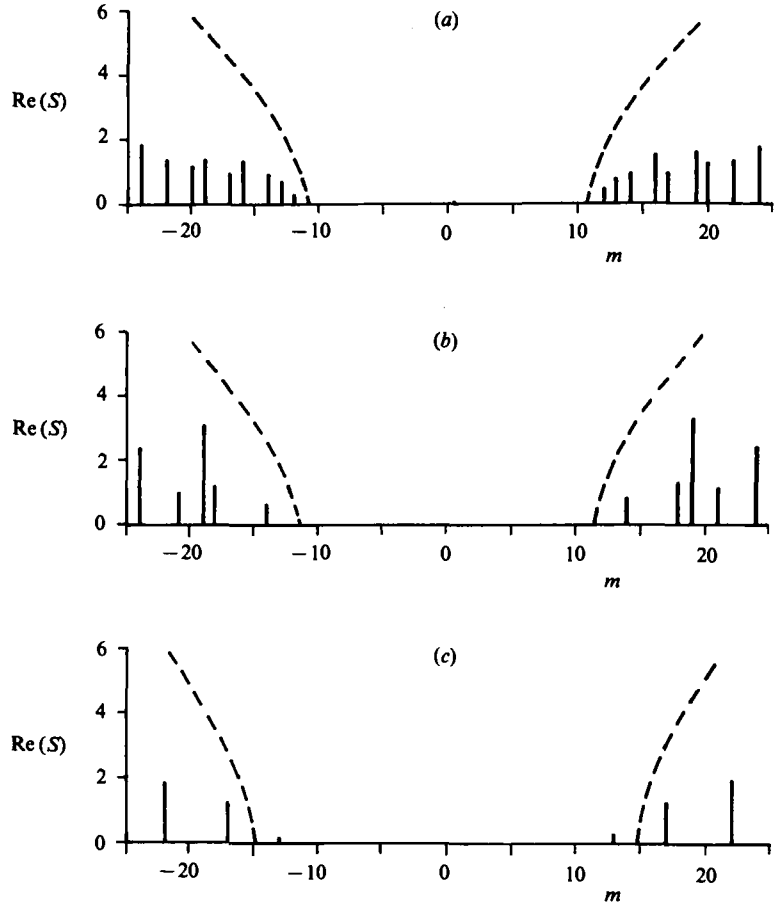

FIGURE 10. Calculated Re (S) spectrum, $D_1 \to \infty$, $\delta = 0.05\pi$, $M = 28$. (*a*) $P = 0.5$, $Q = 0$; (*b*) 0.5, 10; (*c*) 0.5, 30. Vertical bars, calculated spectra; ---, local Kelvin–Helmholtz instability from (4.1).

wave. It can be seen from (4.2) that increasing $|Q|$ inhibits the KH instability, and this is reflected in the results shown in figure 10; most notably, the population of the discrete spectra decreases as $|Q|$ increases. In figure 11 we show the phase speed (i.e. $-\mathrm{Im}\,(S)/(P+2m)$) of the unstable wave-induced KH waves whose growth rates are shown in figure 10(*a*). Again there is reasonable agreement with (4.1). The main wave speed for the case shown is 0.724759677.... Hence the wave-induced KH waves are nearly stationary with respect to the fluid at infinity. The calculated values of m_c from (4.2) for the case $D_1 \to \infty$, $P = 0.5$, $Q = 0$ are $m_c = 250$ ($\delta = 0.01\pi$), $m_c = 41$ ($\delta = 0.025\pi$), $m_c = 10$ ($\delta = 0.05\pi$) and $m_c = 5$ ($\delta = 0.075\pi$). For this same case $\delta_{\max} = 0.188\pi$. Thus the local KH instability sets in for wave amplitudes well below $\delta_{\max}$. Further, since our results indicate that m_c increases as δ decreases, we conclude that this wave-induced KH instability disappears in the limit $\delta \to 0$ (i.e. $\overline{U}_1 - \overline{U}_2 \to 0$, $m_c \to \infty$ as $\delta \to 0$). This contrasts strongly with the KH instability discussed by Yuen (1983), which may in general be attributed to the basic current jump ($\overline{u}_1 \neq 0$) at the interface when $\delta = 0$. Our wave-induced KH instability may be related, however, to the 'nonlinear mode-jumping' phenomenon observed by Yuen in one case (see his figure 4*g*), and which he interpreted as being due to the effect of finite amplitude on the basic KH instability.

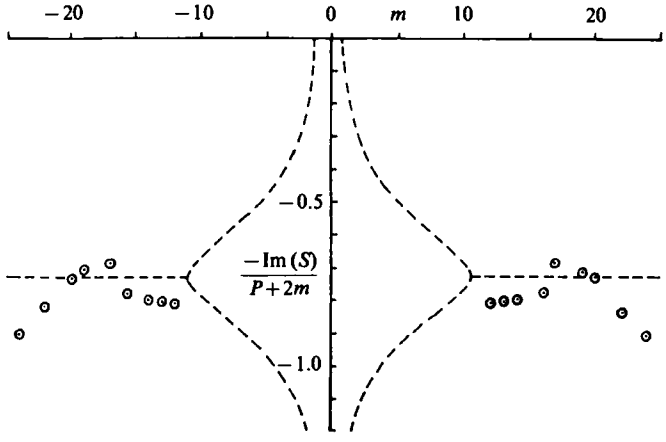

FIGURE 11. Im (S) spectrum plotted as phase speed for that part of spectrum with Re $(S) \neq 0$. $D_1 \to \infty$, $\delta = 0.05\pi$, $P = 0.5$, $Q = 0$, $M = 28$. ⊙, Numerical; ---, (4.1). Main wave speed = 0.724759677....

5. Conclusions

We have shown that, for small to moderate wave amplitudes, interfacial waves are subject to essentially the same hierarchy of three-dimensional resonant instabilities that have been identified for surface gravity waves. The mechanism of the instability can be interpreted as the resonant interaction of two sideband infinitesimal waves with N components of the basic wave where $N \geqslant 2$. Further, the $N = 2$ resonance band incorporates the modulational instability studied in Part 1.

The particular case studied here is the stability of interfacial waves at the interface between two fluids when the lower layer is infinitely deep, using the Boussinesq approximation. We investigated both the $N = 2$ and $N = 3$ instabilities, but for small to moderate wave amplitudes we have found that the $N = 2$ instability dominates. This has a bandwidth $O(\delta)$ and growth rates $O(\delta^2)$ for small wave amplitudes δ, while the $N = 3$ instability has growth rates $O(\delta^3)$. When the upper layer is also infinitely deep the $N = 3$ instability was too weak to be detected. When D_1, the upper-layer depth, is decreased we find that the $N = 2$ instability at first weakens but then grows again, while the $N = 3$ instability becomes stronger (but is always weaker than the $N = 2$ instability).

For larger values of the wave amplitude δ we find that the dominant instability mechanism is a local wave-induced KH instability. This sets in at wave amplitudes generally much less than $\delta_{\max}$, the maximum basic wave amplitude. The numerical evidence suggests this is always present at sufficiently high wavenumbers for all $\delta > 0$, but that it appears in the tail of the discrete eigenvalue spectrum only when the truncation wavenumber M exceeds a threshhold value. In reality, this KH instability would be further restricted or eliminated, by such effects as finite layer thickness between the two fluids, or by such effects as friction and surface tension at the interface. We thus suggest that the KH instability should primarily be viewed as a result of the vortex-sheet model of the basic wave that we have used. However, we note that there is some observational evidence for KH instability in regions of wave-induced shear intensification (see e.g. Woods 1968; Browning 1971; Thorpe *et al.* 1977). Nevertheless, by analogy with the known behaviour of water waves (see e.g. Melville 1982; Su 1982; Su *et al.* (1982)), it seems likely that the resonant-instability

mechanism identified here is the appropriate mode to describe the time evolution of interfacial waves of small or moderate amplitude.

Appendix A. The Boussinesq approximation

In §1 of Part 1 we indicated that one of the motivations for the present study was the prevalance of large-amplitude internal waves on the oceanic pycnocline. However, in the two-layer models discussed in Part 1 and this paper, we have replaced the oceanic free surface with a rigid lid. For the small density differences that occur across the oceanic pycnocline it is well known that this is a valid approximation for linear internal waves. Here we wish to show that it is also a dynamically self-consistent approximation which can be justified *a posteriori* for the finite-amplitude waves and their perturbations considered here.

We consider a two-layer fluid with a lower rigid boundary at $y = -d_2$, an interface at $y = \eta$ separating a fluid of density ρ_1 from a fluid of density ρ_2, and a free surface at $y = d_1 + \zeta$. Using the same notation employed in Part 1 (§2), we assume irrotational flow in each layer with velocity potential ϕ_j and velocity fields $\boldsymbol{u}_j = \nabla\phi_j$. For simplicity we are assuming that there is no basic flow $\bar{u}_j$ in either fluid. The boundary conditions at $y = \eta$ are given in Part 1 ((2.1 and (2.2)). The boundary condition at $y = d_1 + \zeta$ is

$$\frac{\partial\zeta}{\partial t} + u_1\frac{\partial\zeta}{\partial x} + w_1\frac{\partial\zeta}{\partial z} = v_1 \quad \text{on } y = d_1 + \zeta, \tag{A 1a}$$

$$\frac{\partial\phi_1}{\partial t} + \tfrac{1}{2}|\boldsymbol{u}_1|^2 + g\zeta = 0 \quad \text{on } y = d_1 + \zeta. \tag{A 1b}$$

We now introduce dimensionless coordinates based on a lengthscale λ/π and timescale $(\lambda/\pi\alpha g)^{\frac{1}{2}}$, where $\alpha = (\rho_2 - \rho_1)/(\rho_2 + \rho_1)$ is the Boussinesq parameter, and $\alpha \to 0$ in the Boussinesq approximation. Using the same notation for the dimensionless variables described in §2, we find that (A 1*a*, *b*) become

$$\frac{\partial\zeta}{\partial T} + U_1\frac{\partial\zeta}{\partial X} + W_1\frac{\partial\zeta}{\partial Z} = V_1 \quad \text{on } Y = D_1 + \zeta, \tag{A 2a}$$

$$\alpha\left(\frac{\partial\Phi_1}{\partial T} + \tfrac{1}{2}|\boldsymbol{U}_1|^2\right) + \zeta = 0 \quad \text{on } Y = D_1 + \zeta. \tag{A 2b}$$

The interface conditions become (2.1*a*, *b*) and

$$(1+\alpha)\left(\frac{\partial\Phi_2}{\partial T} + \tfrac{1}{2}|\boldsymbol{U}_2|^2\right) - (1-\alpha)\left(\frac{\partial\Phi_1}{\partial T} + \tfrac{1}{2}|\boldsymbol{U}_1|^2\right) + 2\eta = 0 \quad \text{on } Y = \eta. \tag{A 3}$$

We now seek a formal expansion in powers of α. Thus

$$\left.\begin{aligned}\eta &= \eta^{(0)} + H^{(1)} + \dots,\\ \zeta &= \zeta^{(0)} + \alpha\zeta^{(1)} + \dots,\end{aligned}\right\} \tag{A 4}$$

with similar expansions for Φ_j. To leading order $\zeta^{(0)} = 0$ from (A 2*b*) and (A 2*a*) then gives $V_1^{(0)} = 0$ on $Y = D_1$, which is just the rigid-lid boundary condition. Further, $\Phi_j^{(0)}$ and $\eta^{(0)}$ satisfy the interfacial conditions (2.1*a–c*) used in our analysis. Further, from (A 2*b*)

$$\zeta^{(1)} = -\frac{\partial\Phi_1^{(0)}}{\partial T} - \tfrac{1}{2}|\boldsymbol{U}_1^{(0)}|^2. \tag{A 5}$$

For the small to moderate wave amplitudes δ discussed here the right-hand side of (A 5) is $O(1)$. This conclusion remains true when the linearized perturbation terms are superimposed on the basic wave, as even for the unstable waves, the growth rates are $O(\delta^2)$ and remain small for long timescales. Thus $\alpha\zeta^{(1)}$, the leading term in the free-surface displacement is $O(\alpha)$. In the oceanic application α is in the range 10^{-3}–10^{-2}.

Appendix B. Timescale for viscous dissipation

Here we obtain an estimate of the timescale for viscous dissipation of the basic wave for comparison with the growth rate of the calculated resonant instability. We consider interfacial waves propagating on the interface between two fluids of densities ρ_1 and ρ_2 and undisturbed depths d_1 and d_2 in the limit of infinitesimal wave amplitude (i.e. $\delta \to 0$). Explicit expressions for the wave parameters are given in PG*a*. There are four contributions to the viscous dissipation:

(1) dissipation in the interior of the fluid above and below the interface;
(2) dissipation within the unsteady viscous shear layers at the interface;
(3) dissipation within the bottom boundary layer at $y = -d_2$;
(4) dissipation within the top boundary layer at $y = d_1$.

Note that if we regard $y = d_1$ as a free surface, which can be justified in the Boussinesq approximation (see Appendix A), then the contribution (4) can be neglected. To find these contributions we use the method described in Lamb (1932, §§329, 348). Thus we consider the vertically integrated time-averaged energy equation

$$\frac{\partial E}{\partial t} = -\frac{1}{2}\left\langle \int_{-d_2}^{d_1} \mu \left(\frac{\partial u_i}{\partial x_j}\right)^2 \mathrm{d}y \right\rangle, \tag{B 1a}$$

where

$$E = \tfrac{1}{2} g(\rho_2 - \rho_1)\Delta^2. \tag{B 1b}$$

Here 2Δ is the crest-to-trough wave amplitude, and the angle brackets denote a time average; μ is the fluid viscosity and takes the values $\mu_{1,2}$ in each fluid. The contributions to the right-hand side of (B 1*a*) are readily found by standard methods. We find that the decay rate γ due to viscous dissipation is given by

$$-\frac{1}{2E}\frac{\partial E}{\partial t} = \gamma = \gamma_1 + \gamma_2 + \gamma_3 + \gamma_4, \tag{B 2a}$$

where

$$\gamma_1 = 2k^2 \frac{\mu_1 S_1 + \mu_2 S_2}{\rho_1 S_1 + \rho_2 S_2}, \tag{B 2b}$$

$$\gamma_2 = \frac{k(S_1+S_2)^2}{4(\rho_1 S_1 + \rho_2 S_2)} \frac{(2\rho_1\rho_2\mu_1\mu_2\omega)^{\frac{1}{2}}}{(\rho_1\mu_1)^{\frac{1}{2}} + (\rho_2\mu_2)^{\frac{1}{2}}}, \tag{B 2c}$$

$$\gamma_3 = \frac{k\rho_2(S_2^2-1)}{2(\rho_1 S_1 + \rho_2 S_2)} \left\{\frac{\mu_2\omega}{2\rho_2}\right\}^{\frac{1}{2}}, \tag{B 2d}$$

$$\gamma_4 = \frac{k\rho_1(S_1^2-1)}{2(\rho_1 S_1 + \rho_2 S_2)} \left\{\frac{\mu_1\omega}{2\rho_1}\right\}^{\frac{1}{2}}, \tag{B 2e}$$

$$\omega^2 = \frac{gk(\rho_2-\rho_1)}{(\rho_1 S_1 + \rho_2 S_2)}, \quad S_j = \coth kd_j \quad (j = 1, 2). \tag{B 2f}$$

Here $\gamma_1, \ldots, \gamma_4$ are the decay rates due to the contributions (1), ..., (4). In the limit kd_1, $kd_2 \to \infty$ it is readily shown that this expression for γ agrees with that obtained

by Harrison (1908); also we note that when $\rho_1 = 0$ our expression for γ reduces to the well-known result for surface gravity waves. Except in the limit $kd_1, kd_2 \to \infty$ and $\rho_1 \ll \rho_2$, γ_1 may be neglected.

The growth rate of the resonant instability is $s = S(\frac{1}{2}\alpha g k)^{\frac{1}{2}}$, where S is $O((k\Delta)^2)$ and we recall that $\alpha = (\rho_2 - \rho_1)/(\rho_2 + \rho_1)$; S is tabulated in tables 1–3. Next we evaluate γ in the Boussinesq approximation ($\rho_1 \approx \rho_2$) and when the lower fluid is infinitely deep ($kd_2 \to \infty$). In this limit γ_1 and γ_3 can be neglected; we also neglect γ_4 on the grounds that for internal waves in the oceanic pycnocline the upper surface is free and the dissipation there will be negligible compared with that from the interface. We also take $\mu_1/\rho_1 = \mu_2/\rho_2 = \nu$; then γ_2/s is a function of $D_1 = \frac{1}{2}kd_1$, $(k^3\nu^2/\alpha g)^{\frac{1}{4}}$ and S. For a typical wave in the oceanic pycnocline we may put $\alpha = 10^{-3}$, $\nu = 10^{-6}$ m^2 s^{-1} and choose k to correspond to a wavelength of 500 m. For the case $D_1 \to \infty$ (table 1) we then find that $\gamma_2/s = 0.051$ for $\delta/\pi = 0.01$ and $\gamma_2/s = 0.004$ for $\delta/\pi = 0.05$. For the case $D_1/\pi = 0.1$ (table 3) we find that $\gamma_2/s = 0.032$ for $\delta/\pi = 0.01$ and $\gamma_2/s = 0.003$ for $\delta_1/\pi = 0.05$. Thus, at least for oceanic internal waves of moderate amplitude, viscous dissipation occurs on a much longer timescale than that associated with the resonant instability, and hence may be neglected. For typical internal waves in the laboratory we may choose a wavelength of 50 cm and put $\alpha = 10^{-2}$; this increases γ_2 by a factor of about 100, and viscous dissipation will be significant for small-amplitude waves. Of course, in the laboratory there will also be additional dissipation due to the bottom and sidewall boundary layers.

REFERENCES

Browning, K. A. 1971 Structure of the atmosphere in the vicinity of large-amplitude Kelvin–Helmholtz billows. *Q. J. R. Met. Soc.* **97**, 283–299.

Chen, B. & Saffman, P. G. 1980 Numerical evidence for the existence of new types of gravity waves of permanent form on deep water. *Stud. Appl. Maths* **62**, 1–21.

Garbow, B. S. 1978 Algorithm 535: the *QZ* algorithm to solve the generalized eigenvalue problem for complex matrices. In *Collected Algorithms of ACM*.

Grimshaw, R. H. J. & Pullin, D. I. 1985 Stability of finite-amplitude interfacial waves. Part 1. Modulational instability for small-amplitude waves. *J. Fluid Mech.* **000**, 000–000.

Harrison, W. J. 1908 The influence of viscosity on the oscillation of superposed fluids. *Proc. Lond. Math. Soc.* **6**, 396–405.

Kaufman, L. 1975 Algorithm 496: the *LZ* algorithm to solve the generalized eigenvalue problem for complex matrices. In *Collected Algorithms of ACM*.

Lamb, H. 1932 *Hydrodynamics*, 6th edn. Cambridge University Press.

McLean, J. W. 1982*a* Instabilities of finite-amplitude water waves. *J. Fluid Mech.* **114**, 315–330.

McLean, J. W. 1982*b* Instabilities of finite-amplitude gravity waves on water of finite depth. *J. Fluid Mech.* **114**, 331–341.

McLean, J. W., Ma, Y. C., Martin, D. U., Saffman, P. G. & Yuen, H. C. 1981 Three-dimensional instability of finite-amplitude water waves. *Phys. Rev. Lett.* **46**, 817–820.

Meiron, D. I. & Saffman, P. G. 1983 Overhanging interfacial gravity waves of large amplitude. *J. Fluid Mech.* **129**, 213–218.

Meiron, D. I., Saffman, P. G. & Yuen, H. C. 1982 Calculation of steady three-dimensional deep-water waves. *J. Fluid Mech.* **124**, 109–121.

Melville, W. K. 1982 The instability and breaking of deep-water waves. *J. Fluid Mech.* **115**, 165–185.

Phillips, O. M. 1960 On the dynamics of unsteady gravity waves of finite amplitude. Part 1. The elementary interactions. *J. Fluid Mech.* **9**, 193–217.

Pullin, D. I. & Grimshaw, R. H. J. 1983*a* Nonlinear interfacial progressive waves near a boundary in a Boussinesq fluid. *Phys. Fluids* **26**, 897–905.

PULLIN, D. I. & GRIMSHAW, R. H. J. 1983*b* Interfacial progressive waves in a two-layer shear flow. *Phys. Fluids* **26**, 1731–1739.

SAFFMAN, P. G. & YUEN, H. C. 1980 A new type of three-dimensional deep-water wave of permanent form. *J. Fluid Mech.* **101**, 797–808.

SU, M. Y. 1982 Three-dimensional deep-water waves. Part 1. Experimental measurement of skew and symmetric wave patterns. *J. Fluid Mech.* **124**, 73–108.

SU, M. Y., BERGIN, M., MARLER, P. & MYRICK, R. 1982 Experiments on nonlinear instabilities and evolution of steep gravity-wave trains. *J. Fluid Mech.* **124**, 45–72.

THORPE, S. A., HALL, A. J., TAYLOR, C. & ALLEN, J. 1977 Billows in Loch Ness. *Deep-Sea Res.* **24**, 371–379.

WOODS, J. D. 1968 Wave-induced shear instability in the summer thermocline. *J. Fluid Mech.* **32**, 791–800.

YUEN, H. C. 1983 Instability of finite-amplitude interfacial waves. In *Waves on Fluid Interfaces* (ed. R. E. Meyer), pp. 17–40. Academic.

YUEN, H. C. & LAKE, B. M. 1982 Nonlinear dynamics of deep-water gravity waves. *Adv. Appl. Mech.* **22**, 67–229.